Journal of Geochemical Exploration 176 (2017) 50–56

Contents lists available at ScienceDirect

Journal of Geochemical Exploration

journal homepage: www.elsevier.com/locate/gexplo

Adsorption of lead on organo-mineral complexes isolated from loess in Northwestern China

Chunhui Fan [a,*], Bo Du [a], Yingchao Zhang [b], Shaolan Ding [a], Yalin Gao [a], Min Chang [a]

[a] College of Resource and Environment, Shaanxi University of Science & Technology, Xi'an 710021, China
[b] College of Environment, Tsinghua University, Beijing 100084, China

ARTICLE INFO

Article history:
Received 30 June 2015
Revised 22 January 2016
Accepted 28 February 2016
Available online 2 March 2016

Keywords:
Organo-mineral complexes (OMCs)
Adsorption behavior
Lead
Loess

ABSTRACT

Four types of organo-mineral complex (OMC) samples with different sizes were extracted from loess in northwestern China. OMC, which has a size less than 2 μm, was used to investigate the adsorption behavior of lead. The OMC sample had a porous structure with a surface area of 147.49 m^2/g, and the adsorption capacity changed with different conditions of OMC content, pH values of the solution, temperature, and ionic strength. The adsorption isotherms suggested that the adsorption process was favorable, and the maximum adsorption capacity of lead on OMC was 1.5877 mg/g, which was calculated by using Langmuir equation. The reaction fits better the pseudo-second-order kinetic equation, and the adsorption behavior could be divided into two sections, thereby indicating that the reaction involved physical and chemical adsorption. The adsorption of lead on OMC was spontaneous and exothermic in nature, and the randomness of the system decreased slightly throughout the entire process. The desorption efficiency was acceptable with purified water and with ultrasonic assistance.

1. Introduction

Heavy metal contamination of agricultural soil occurs with rapid urbanization and industrialization, and is attracting increasing public attention in China. Such attention is warranted because the presence of heavy metals in soils might pose a serious threat to human health through the food chain (Chen et al., 2013; Yu et al., 2012). Lead (Pb), as one of the toxic metals that are commonly discovered in agricultural soils, can easily enter the soil system through various approaches, such as atmospheric deposition, sewage irrigation, and application of fertilizers and pesticides (Finster et al., 2004; Huang et al., 2014; Sun et al., 2006). Soil is known to function as a chemical and as a filter that reduces the environmental effect of Pb introduced into the biosphere. The biosphere is the first line of prevention against Pb contamination of groundwater, which occurs partly through the adsorption process. A high level of Pb in soils may affect crop yields significantly, deteriorate soil quality, and inevitably increase the risk of Pb contamination in farm products (Wang et al., 2006). Consequently, an in-depth understanding of the physicochemical behaviors of Pb in soils is necessary.

As the special particle unit of soil, organo-mineral complexes (OMCs) have long been used to study the migration and distribution of organic matter in soils (Feng et al., 2014; Junet and Basile, 2013). Given the small particle size of OMC, the ability of OMC to adsorb foreign substances, including metals, nitrogen and phosphate, might be different from that of other soil constituents because of various characteristics of specific surface area and pore structures (Acosta et al., 2009; Bi et al., 2013). Relevant research on the matter has been completed (Acosta et al., 2009; Bradl, 2004; Dultz et al., 2005); however, most studies focus on coarse particles, such as soil aggregates, clay minerals, and sediments. Investigating the reaction behavior between OMC samples and heavy metals is important.

The main factors that affect the adsorption process include metal speciation and concentration, contact time, temperature, and pH value. pH value is the most important environmental factor because of its strong effect on chemical speciation and solubility of heavy metals (Harter, 1983). The major objective of this paper was to identify the composition and surface structure of OMC isolated from loess in northwestern China and to investigate the relationship between environmental parameters and the adsorption process. This paper also investigates the reaction kinetics, isotherms, and thermodynamics of the adsorption of lead on OMC. This research is significant in improving the understanding of the adsorption mechanism between OMC and Pb, and in further evaluating the transformation behavior of Pb in the pedosphere or ecosystem in a reasonable manner.

2. Materials and methods

2.1. Isolation of OMC

Loess samples were collected from a 0–20 cm deep surface horizon of farmland located in Shaanxi University of Science and Technology, Xi'an, China. The samples were transported to the laboratory in polyethylene bags and divided into four subsamples through the sedimentation

* Corresponding author.
E-mail address: fanchunhui@sust.edu.cn (C. Fan).

http://dx.doi.org/10.1016/j.gexplo.2016.02.012
0375-6742/

method. The division of the subsamples is as follows: <2 μm particles, 2–20 μm particles, 20–200 μm particles and >200 μm particles (Bradl, 2004). The <2 μm particles were used in the study, and all samples were air dried and kept in a desiccator over silica gel for subsequent utilization.

2.2. Physicochemical analysis of OMC

The composition of OMC was determined by chemical analysis. A Brunauer–Emmett–Teller (BET) surface analyzer (Nova2200e, QUANTACHROME) was used to measure nitrogen adsorption at 77 K. The surface area of OMC was calculated from the isotherms by using the BET equation. The mineral phases of OMC were revealed with an X-ray diffractometer (D/max2200PC, RIGAKU) that ran at 40 kV and 40 mA by using a Cu Kα radiation. The surface morphology of OMC was identified by using a scanning electron microscope (TM1000, HITACHI). The Fourier transform infrared (FT-IR) spectra were obtained in the range of 4000–400 cm^{-1} on a spectrometer (Vector22, BRUKER) with KBr pellet method at room temperature.

2.3. Adsorption studies

A stock solution of 1000 mg/L of Pb was prepared from $Pb(NO_3)_2$. Experimental solutions of the desired concentration were obtained by diluting the stock solution using purified water. The effects of OMC content, original pH value of solution, temperature, and ionic strength on adsorption behaviors were investigated. A constant-temperature air bath shaker (ZD-85, Changzhou, China) was used to control the desired temperature. The pH values of solution were adjusted by adding HCl or NaOH solutions. All pH measurements were performed by using a pH meter (pHS-3C, Shanghai, China).

The OMC sample was placed in a 250 mL conical flask with a stopper; the flask contained 20 mL of the experimental solution of known concentration. The suspensions were shaken at 120 rpm for 4 h. The supernatant liquids were then centrifuged at 4000 rpm for 5 min and then filtered with 0.45 μm filter. All the experiments were performed for three times. The initial and final concentrations of Pb were measured by using a flame atomic adsorption spectrometer (Z-2000, HITACHI). The obtained data were applied to calculate the adsorption capacity (q_e, mg/g) by using the following relationship:

$$q_e = (C_0 - C_e)/m \times V. \quad (1)$$

The removal efficiency (%) of lead on OMC can be calculated as follows:

$$Removal\ efficiency(\%) = (C_0 - C_e)/C_0 \times 100 \quad (2)$$

where C_0 and C_e (mg/L) are the initial and equilibrium concentrations of Pb, respectively, V (mL) is the volume of the solution, and m (mg) is the content of OMC.

2.4. Desorption studies

Desorption experiments were carried out by using purified water as a desorbing agent with ultrasonic assistance. The effect of the different volumes of purified water (50, 100, 150 and 200 mL) and ultrasound power (25, 50, 75 and 100 W) on desorption efficiency was studied by contacting 0.1 g of Pb-loaded OMC samples. The mixture was stirred until desorption equilibrium was achieved at 25 °C and then filtered. The concentration of desorbed Pb in the filtrate was checked. The desorption efficiency of Pb was calculated by using the following equation:

$$Desorption\ efficiency(\%) = C_d V_d / q_e m \times 100 \quad (3)$$

where C_d (mg/L) is the concentration of Pb in the purified water at desorption equilibrium, V_d (L) is the volume of purified water, m(g) is the mass of OMC used for desorption studies, and q_e (mg/g) is the adsorption capacity of OMC for Pb.

3. Results and discussion

3.1. Characterization of OMC

3.1.1. BET and XRD

The BET surface area of OMC derived from loess was 147.49 m^2/g, which is lower than that of the loess sample described in our previous investigation (Fan et al., 2013), thereby indicating acceptable adsorption sites on OMC samples. The XRD pattern of OMC is shown in Fig. 1. The crystal phase of the OMC was mainly composed of quartz (26.64°), muscovite (34.94°), clinochlore (19.80°), and polylithionite (27.94°). Results showed that the clay minerals of the OMC were poorly organized, and many disoriented particles were stacked randomly.

3.1.2. SEM

To determine some physical characteristics of the surface morphology of OMC, a morphological investigation was conducted by SEM. Fig. 2 displays the SEM images of OMC, and micrometric particles of different sizes could be observed. The surface of the OMC, which involved a majority of tiny pores, was clearly uneven.

3.1.3. FT-IR

The nature of OMC surface configuration was examined by spectroscopic analyses, and the FT-IR spectra are presented in Fig. 3. In the spectra, the typical bands at 3471 and 3416 cm^{-1} were related to the stretching vibration of O–H groups likely indicating the presence of H_2O in the OMC. A band within the 1620–1639 cm^{-1} region was also visible and might be attributed to CONH or the bending vibration of the hydroxyl and interlayer water molecules. The peak recorded at 1452 cm^{-1} might be attributed to carbonate, and a band at 877 cm^{-1} could be attributed to Si–O bending vibrations.

3.2. Adsorption process

3.2.1. Influential factors

3.2.1.1. Effect of OMC content on lead adsorption. The effect of OMC content on lead adsorption was studied by changing the OMC content from 0.01 to 0.4 g at room temperature; results are presented in Fig. 4. The removal rate increased evidently from 5.05 to 92% within the OMC content from 0.01 up to 0.2 g and remained nearly constant thereafter. This condition occurred because the number of available

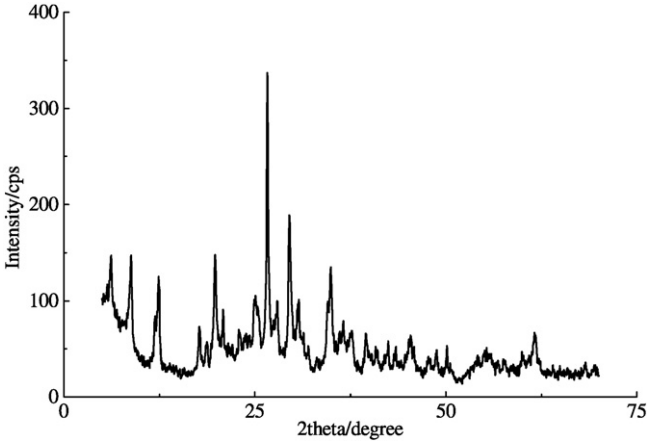

Fig. 1. The X-ray diffraction pattern of OMC samples.

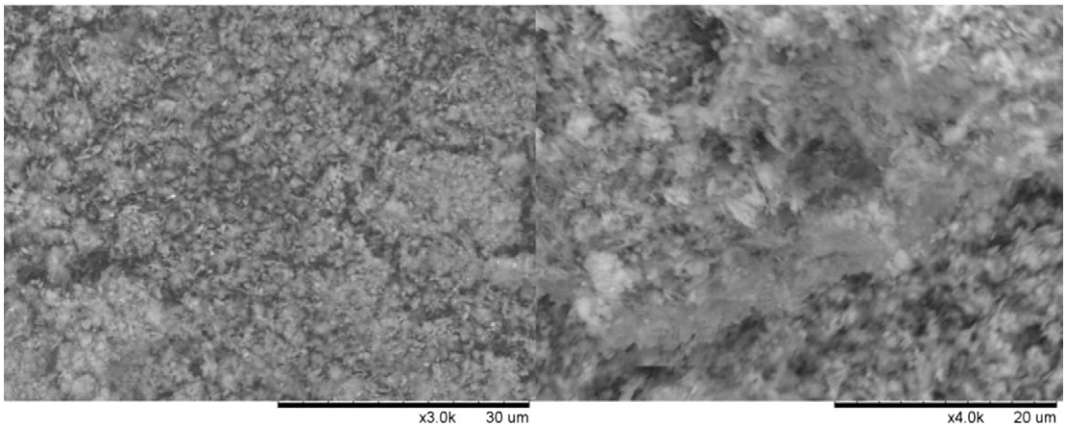

Fig. 2. SEM micrographs of OMC.

adsorption sites increased by increasing the OMC content. However, the adsorption capacity decreased gradually mainly because of unsaturated adsorption sites throughout the adsorption reaction (Kadirvelu and Namasivayam, 2003). Particle interaction, such as aggregation, may decrease the total surface area of the adsorbent, and this decrease may be the reason for the reduced adsorption capacity.

3.2.1.2. Effect of pH values on lead adsorption. The pH value of the solution plays an important role in the adsorption process (Anbia and Ghassemian, 2011; Gao et al., 2010; Ren et al., 2013), because it not only affects the surface charge of the adsorbent but also determines the ionization degree and speciation of heavy metals (Deng and Ting, 2005; Park et al., 2010). The influence of pH values on lead adsorption was studied from pH ranges of 4.0–9.0, and results are shown in Fig. 5. The adsorption capacity of lead on OMC increased as the pH values increased from 4.0 to 7.5, peaking at 1.03 mg/g when the pH value was 7.5. Afterwards, the adsorption capacity no longer continued to increase, but rather, it decreased gradually. Dominant lead species were diverse at different pH values. When the pH value was less than 7.5, the predominant lead species was Pb(II), and the adsorption process occurred easily. Moreover, at lower pH, the concentration of H^+ ions was high, which interfered with the adsorption of metal ions directly. The active sites of the adsorbent were protonated excessively, thereby reducing the adsorption capacity if the metal ions reduced (Kumar et al., 2009). However, a detail that should be noted is that OMC is regarded as a complex component more than as an organic colloid or inorganic colloid, or an organic colloid and inorganic colloid. The environmental factors and the adsorption process itself in the solution might change or destroy the micro-characteristics of OMC, such as the amount of functional groups on OMC surface, pore structure, specific surface area, and surface charge density (Feng et al., 2014). The related behaviors and effects are complicated possibly leading to the different adsorption characteristics of lead on OMC. In this paper, the acceptable pH value was 7.5.

3.2.1.3. Effect of temperature on lead adsorption. Experiments were performed at eight different temperatures to explore the relationship between temperature and the adsorption capacity of lead on OMC. The maximum adsorption amount (1.06 mg/g) was attained at 303 K; beyond this temperature, the adsorption capacity decreased slightly, as shown in Fig. 6. The high temperature had little influence on the adsorption capacity of lead on OMC; however, when the temperature was below 303 K, the adsorption amount decreased to some extent to a minimum of 0.92 mg/g at 293 K; this decrease demonstrated a drop of 13%. This finding indicates that raising the temperature favors lead adsorption to some extent.

3.2.1.4. Effect of ionic strength on lead adsorption. Experiments were carried out in the presence of different anion concentrations of chloride ion, nitrate ion, and phosphate ion under identical conditions to assess the influence of anions on the adsorption of lead on OMC; results are summarized in Fig. 7. As ionic strength, including chloride ion, nitrate ion, and phosphate ion, increased from 0 to 0.2 mg/L, the extent of lead adsorption onto OMC decreased obviously, and the degree of influence almost did not exhibit any differences. The adsorption amounts of lead, which were 0.78, 0.72, and 0.66 mg/g, differed markedly as the anion concentrations increased to 0.2 mg/L. A possible explanation for this phenomenon might be the theory of electrical double layer. According to this theory, when OMC and Pb were in contact with each other, they were bound to be encircled by an electrical double layer because

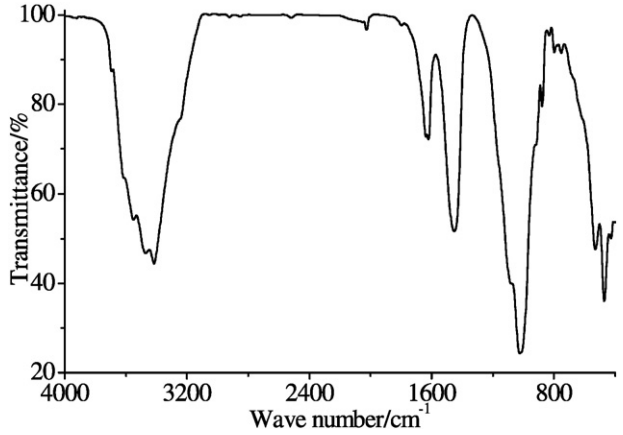

Fig. 3. The FT-IR spectra of OMC.

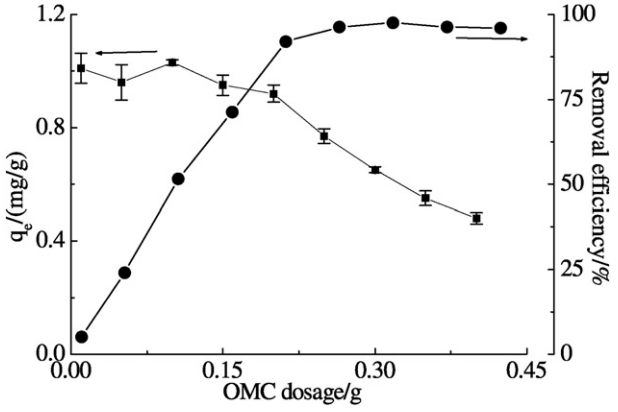

Fig. 4. Effect of OMC content for Pb adsorption on OMC. Adsorption experiments—C_0: 10 mg/L; pH: 7; temperature: 298 K; solution volume: 20 mL.

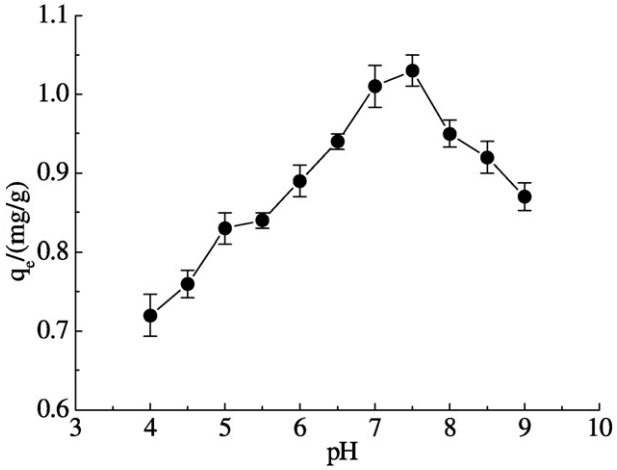

Fig. 5. Effect of pH for Pb adsorption on OMC. Adsorption experiments—C_0: 10 mg/L; sample dose: 0.1 g/20 mL; temperature: 298 K.

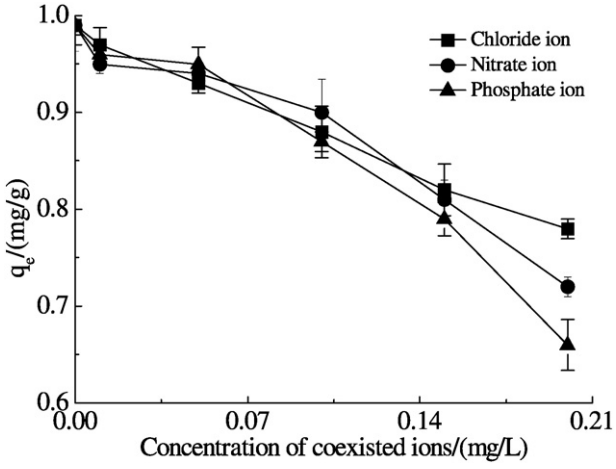

Fig. 7. Effect of ion concentration of chloride, nitrate and phosphate for Pb adsorption on OMC. Adsorption experiments—C_0: 10 mg/L; pH: 7; sample dose: 0.1 g/20 mL; temperature: 298 K.

of electrostatic interaction, and the electrostatic attraction decreased with increasing ionic strength; thus, the adsorption capacity reduced. In addition, some anions might form complexes with metal ions and interfere with the adsorption process (Ajmal et al., 1998) as a result. The effect of ionic strength could assist in making a distinction between the inner-sphere and outer-sphere surface complexes (Lützenkirchen, 1997). The inner-sphere complexes were hardly affected by the ionic strength, whereas outer-sphere complexation was significantly decreased by increasing ionic strength. Therefore, the adsorption process of lead onto OMC could be inferred to have proceeded in light of outer sphere complexation.

3.2.2. Adsorption isotherm

Adsorption isotherm studies can better interpret the relationship between equilibrium adsorption capacity and equilibrium concentration at a definite temperature. The adsorption isotherms of lead on OMC within the volume of the solution were 20 mL, the mass of OMC was 0.02 g, and the lead concentration ranged from 0.2 to 2.0 mg/L at 25 °C; these parameters were studied, and results are presented in Fig. 8. The adsorption capacity of Pb increased obviously with the increase of equilibrium concentration. In this study, the adsorption equilibrium data were analyzed by using the Langmuir and Freundlich adsorption isotherm models. The Langmuir model was believed to be suitable for homogeneous adsorption where the adsorption process had identical activation energy and was applicable to monolayer adsorptions that did not have any interaction between metal ions (Abdullah et al., 2009). The Langmuir equation is given as follows:

$$C_e/q_e = C_e/q_m + 1/q_m K_L \tag{4}$$

where C_e (mg/L) is the equilibrium concentration of Pb, q_e (mg/g) is the adsorption capacity at equilibrium, and K_L (L/mg) and q_m (mg/g) are the Langmuir constants involved in adsorption energy and saturated adsorption capacity, respectively. The Langmuir isotherm parameters q_m and K_L were calculated from slope $(1/q_m)$ and intercept $(1/K_L q_m)$ of the plot of C_e/q_e versus C_e, respectively, and the correlative data are given in Table 1. The value of correlation coefficient ($R^2 = 0.9875$) was close to 1, which indicated that the Langmuir model was suitable for Pb adsorption onto OMC. Moreover, the separation factor (R_L) that assessed the feasibility of adsorption on adsorbent was an important parameter, and its equation is defined as follows:

$$R_L = 1/(1 + K_L C) \tag{5}$$

where K_L (L/mg) is the Langmuir constant, C (mg/L) is the initial ion concentration of Pb, and the concrete values of R_L could help to

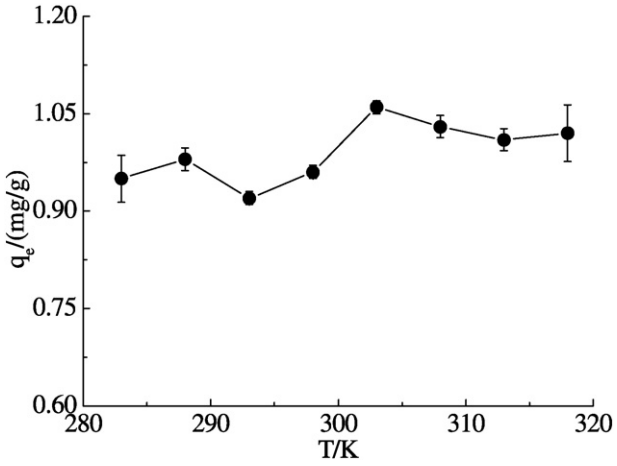

Fig. 6. Effect of temperature for Pb adsorption on OMC. Adsorption experiments—C_0: 10 mg/L; pH: 7; sample dose: 0.1 g/20 mL.

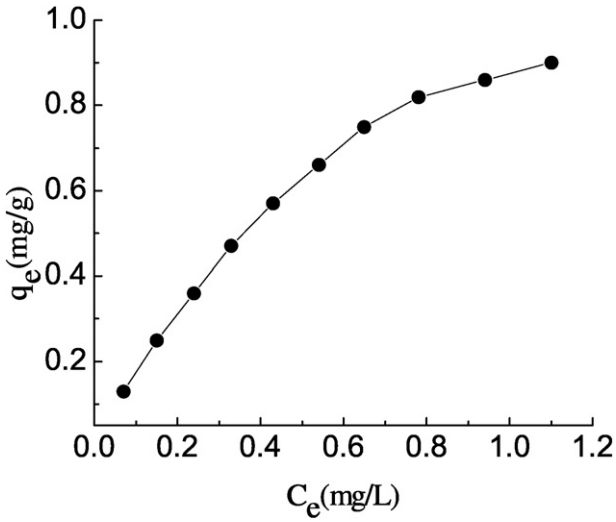

Fig. 8. The adsorption isotherm of Pb on OMC.

Table 1
The Langmuir and Freundlich equations and parameters for the adsorption of Pb on OMC.

Langmuir model				Freundlich model		
K_L(L/mg)	q_m(mg/g)	R^2	R_L	K_F(mg/g)	n(g/L)	R^2
1.2805	1.5877	0.9875	0.2808–0.7961	0.9664	1.3976	0.9828

distinguish the type of the isotherm: unfavorable ($R_L > 1$), linear ($R_L = 1$), favorable ($R_L < 1$), and irreversible ($R_L = 0$) (Sharma et al., 2010), which are displayed in Table 1. Results suggested that Pb adsorption onto OMC was favorable.

Unlike the Langmuir model, the Freundlich model describes multilayer adsorptions on the heterogeneous surface (Zhen et al., 2013). The Freundlich equation is given as follows:

$$logq_e = logK_F + logC_e/n \tag{6}$$

where q_e (mg/g) is the adsorption capacity at equilibrium, C_e (mg/L) is the equilibrium concentration of Pb, and n (g/L) and K_F (mg/g) reflect the affinity of OMC to metal ions, and their values were obtained from slope ($1/n$) and intercept ($logK_F$) of the plot of $logq_e$ versus $logC_e$, respectively; the detailed parameters are summarized in Table 1. As seen from Table 1, the correlation coefficient value obtained from the Langmuir model ($R^2 = 0.9875$) was similar to that calculated from the Freundlich model ($R^2 = 0.9828$), thereby suggesting that both the Langmuir model and Freundlich model could illustrate the adsorption process. However, the value of n indicates the favorability of adsorption; in this study, $n > 1$ demonstrated that the adsorption was favorable (Wang et al., 2010). This finding is consistent with the conclusion of the Langmuir model.

3.2.3. Adsorption kinetics

Adsorption kinetics could clarify the adsorption rate of Pb on OMC at a certain initial temperature (25 °C) and confirms the adsorption time from the beginning to equilibrium. As shown in Fig. 9, the adsorption capacity increased with the extension of contact time. Obviously, in the first 75 min, the adsorption was rapid and then slowed significantly. The probable interpretation for this condition is that Pb ions might easily enter the accessible pore sites and bound with the chelating ligands in the initial fast adsorption step, while in the following slow adsorption step, some Pb ions might penetrate into the deeper pores.

To explore the related diffusion mechanism during the adsorption process, the pseudo-first-order kinetic and pseudo-second-order kinetic models (Ghasemi et al., 2014) were studied. These models could be defined by Eqs. (7) and (8), respectively.

$$\log(q_e - q_t) = logq_e - k_1 t/2.303 \tag{7}$$

$$t/q_t = 1/k_2 q_e^2 + t/q_e \tag{8}$$

where q_e (mg/g) is the adsorption capacity at equilibrium; q_t (mg/g) represents the amounts of Pb adsorbed at time t (min); and k_1 (min^{-1}) and k_2 (g/mg min) are the rate constants of pseudo-first-order and pseudo-second-order kinetic equations, respectively. k_1 and $q_{e\ cal}$ are computed by plotting $log(q_e\text{-}q_t)$ against t, and the plot of t/q_t versus t allowed calculation of the rate constant k_2 and $q_{e\ cal}$. The calculated and experimental q_e values, and k_1, k_2, the correlation coefficient (R^2) values, are listed in Table 2. The correlation coefficient (R^2) values of two kinetic models are almost equal. However, a comparison with $q_{e\ cal}$ values of two kinetic models indicates that the $q_{e\ cal}$ value of the pseudo-first-order model was obviously much closer to $q_{e\ exp.}$ value. This finding indicates that the pseudo-second-order model was more suitable than the pseudo-first-order model for Pb removal on OMC.

3.2.4. Intra-particle diffusion model

The obtained adsorption isotherms and kinetics indicate that the adsorption process of Pb on OMC involved physical and chemical adsorption. The intra-particle diffusion equation was used to illustrate the reaction to further reveal the adsorption mechanism and diffusion behavior of Pb on OMC (Weber and Morris, 2015). The equation is described as follows:

$$Q_t = k_t t^{0.5} + I \tag{9}$$

where Q_t (mg/g) is the adsorption capacity at t, k_t (mg/g/$min^{-0.5}$) is the intra-particle diffusion rate constant, and I (mg/g) is the intercept related to interface characteristics.

The adsorption process of Pb on OMC could be generally divided into two sections, as shown in Fig. 10. The initial section might be attributed to external surface adsorption, in which Pb diffuses through the solution to the external surface of OMC, where the adsorption rate is high. The second section describes the gradual adsorption stage, in which the intra-particle diffusion starts to slow down and intraparticle diffusion rate is rate controlling. None of the lines passed through the origin, which proves that intraparticle diffusion was involved in the adsorption process, but was not the only rate-controlling step.

3.2.5. Adsorption thermodynamics

Adsorption thermodynamics could reveal the effects of the energy in the adsorption process and also confirms whether an adsorption process could occur under a certain temperature and conditions. Adsorption thermodynamics studies were conducted at different temperatures (283, 288, 293, 298, 303, and 308 K). Thermodynamics parameters, including Gibbs free energy (ΔG^0), enthalpy change (ΔH^0), and entropy change (ΔS^0), were calculated through the following equations.

$$\Delta G^0 = -RTlnK_0 \tag{10}$$

$$lnK_0 = \Delta S^0/R - \Delta H^0/RT \tag{11}$$

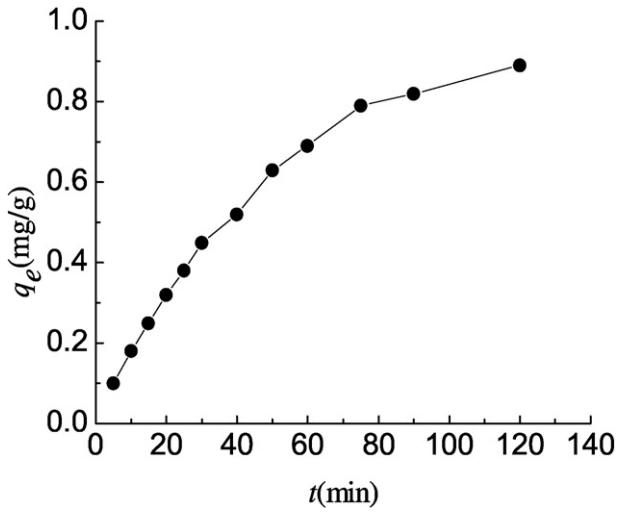

Fig. 9. Adsorption kinetics of Pb on OMC.

Table 2
The pseudo-first-order and pseudo-second-order equations and parameters for the adsorption of Pb on OMC.

$q_{e\ exp.}$	Pseudo-first-order kinetic			Pseudo-second-order kinetic		
(mg/g)	k_1(min^{-1})	$q_{e\ cal}$ (mg/g)	R^2	k_2(g/mg min^{-1})	$q_{e\ cal}$ (mg/g)	R^2
1.05	0.0162	0.9938	0.9885	0.0102	1.4385	0.9895

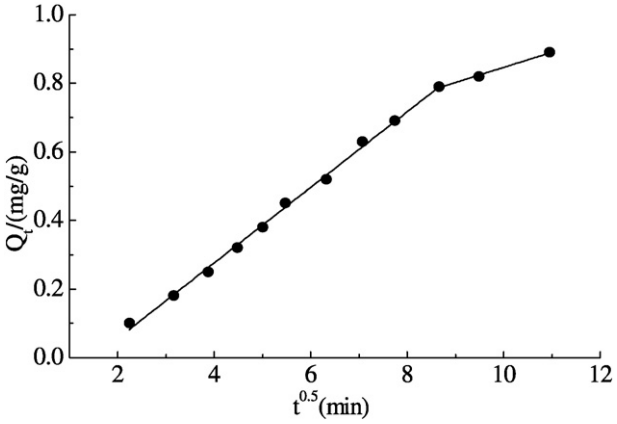

Fig. 10. Intra-particle diffusion model for adsorption of Pb on OMC.

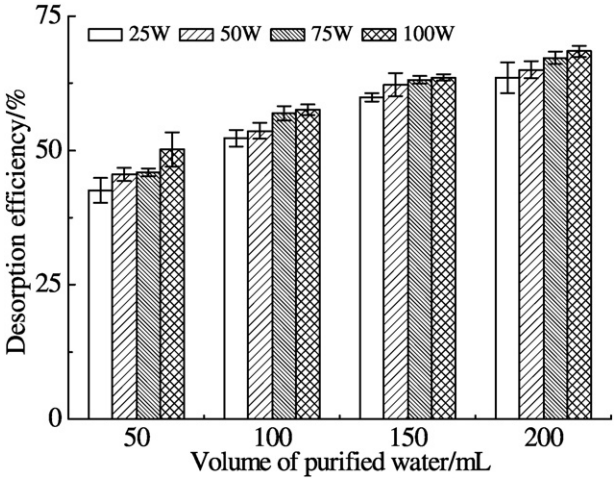

Fig. 11. Desorption effect of Pb from OMC under different conditions.

where K_0 is the distribution coefficient of different temperatures, R (8.314 J/mol K) represents the molar gas constant, T (K) is the absolute temperature, and ΔH^0 and ΔS^0 are computed from the slope and intercept of the linear plot of InK_0 versus $1/T$. All data are shown in Table 3. The negative value of ΔG^0 demonstrates that the adsorption of Pb ions onto OMC was feasible and spontaneous in the range of experimental temperature. In addition, with respect to the adsorption process, the absolute value of ΔH^0 was lower than 40 kJ/mol, which illustrated that this adsorption process was controlled by a physical mechanism rather than a chemical mechanism. In this paper, the value of ΔH^0 (−3.5884 kJ/mol) clearly indicates that the adsorption was exothermic. The value of ΔS^0 presented an idea to depict the randomness at the solid–solution interface during the adsorption process. The negative value of ΔS^0 (−0.0565 kJ/mol K) proved the decrease of randomness.

3.3. Desorption

In general, desorption behavior was investigated to provide insight into potential adsorption mechanisms between adsorbents and solutes. Thus, studying the desorption of Pb from OMC was necessary. The same parameters, except for the volume of purified water and ultrasound power, were used in the desorption experiment. Experimental results showed the desorption efficiency of Pb, and the data are listed in Fig. 11. As observed, with the volume of purified water constant kept constant, the desorption efficiency of Pb increased with increasing ultrasound power from 25 W to 100 W. This phenomenon might be due to the emergence of more cavitation events with high power. As a result, more Pb ions were desorbed from OMC. The increase of ultrasound power corresponds to an increase in the acoustic amplitude, a higher acoustic amplitude, and a more violent cavitation bubble collapse. Thus, the higher power would result in greater ultrasonic effects in the collapsing bubble. Consequently, high ultrasound power could be concluded to break the bonds between Pb and OMC, and enhance the mass transfer through high-pressure shock waves, high-speed microjets, and acoustic vortex microstreaming (Hamdaoui and Naffrechoux, 2007). The desorption efficiency of Pb could increase only by increasing the volume of purified water, thereby indicating that physical adsorption must have played a major role in the adsorption process (Meitei and Prasad, 2013). This finding is consistent with the results of adsorption thermodynamics.

Table 3
Thermodynamic parameters for the adsorption of Pb ions onto OMC.

T(K)	283	288	293	298	303	308
ΔG^0(kJ/mol)	−1.2525	−1.2028	−1.1531	−1.1034	−1.0537	−1.0040
ΔH^0(kJ/mol)				−3.5884		
ΔS^0(kJ/mol K)				−0.0565		

4. Conclusions

In this paper, OMCs were extracted from loess samples in northwestern China. The adsorption characteristics and mechanisms of Pb on OMC were discussed in batch adsorption procedures. OMC has a porous structure with a surface area of 147.49 m^2/g. The adsorption capacity of Pb on OMC reached its maximum at a pH value of 7.5, and the adsorption capacity changes with various conditions of OMC dosage, temperature, and ionic strength. The Langmuir and Freundlich isotherms fit the adsorption process acceptably, and the maximum adsorption capacity was 1.5877 mg/g, as calculated from the Langmuir isotherm. The pseudo-second-order kinetic equation fit the reaction well, and the adsorption process was spontaneous and exothermic. The desorption efficiency was acceptable with purified water and in an ultrasonic assisted system. Results reveal the physicochemical effect in the Pb removal process on OMC.

Acknowledgments

This work was supported by the National Natural Science Foundation of China (No. 21407103) and the Postdoctoral Science Foundation of China (No. 2012 M511968).

References

Abdullah, M.A., Chiang, L., Nadeem, M., 2009. Comparative evaluation of adsorption kinetics and isotherms of a natural product removal by amberlite polymeric adsorbents. Chem. Eng. J. 146, 370–376.
Acosta, J.A., Cano, A.F., Arocena, J.M., Debela, F., Martínez-Martínez, S., 2009. Distribution of metals in soil particle size fractions and its implication to risk assessment of playgrounds in Murcia City (Spain). Geoderma 149, 101–109.
Ajmal, M., Khan, A.H., Ahmad, S., Ahmad, A., 1998. Role of sawdust in the removal of copper(II) from industrial wastes. Water Res. 32, 3085–3091.
Anbia, M., Ghassemian, Z., 2011. Removal of Cd(II) and Cu(II) from aqueous solutions using mesoporous silicate containing zirconium and iron. Chem. Eng. Res. Des. 89, 2770–2775.
Bi, X., Liang, S., Li, X., 2013. A novel in situ method for sampling urban soil dust: particle size distribution, trace metal concentrations, and stable lead isotopes. Environ. Pollut. 177, 48–57.
Bradl, H.B., 2004. Adsorption of heavy metal ions on soils and soils constituents. J. Colloid Interface Sci. 277, 1–18.
Chen, W., Lu, S., Chi, P., Jiao, W., Wang, M., 2013. Accumulation of Cd in agricultural soil under long-term reclaimed water irrigation. Environ. Pollut. 178, 294–299.
Deng, S., Ting, Y.P., 2005. Characterization of PEI-modified biomass and biosorption of Cu(II), Pb(II) and Ni(II). Water Res. 39, 2167–2177.
Dultz, S., Riebe, B., Bunnenberg, C., 2005. Temperature effects on iodine adsorption on organo-clay minerals: II. Structural effects. Appl. Clay Sci. 28, 17–30.
Fan, C.H., He, L., Zhang, Y.C., Wang, J.H., 2013. Spectral identification of fingerprint spectrum of loess of arid farmland in Northwest China. Spectrosc. Spectr. Anal. 33, 1697–1700.

Feng, W., Plante, A.F., Aufdenkampe, A.K., Six, J., 2014. Soil organic matter stability in organo-mineral complexes as a function of increasing C loading. Soil Biol. Biochem. 69, 398–405.
Finster, M.E., Gray, K.A., Binns, H.J., 2004. Lead levels of edibles grown in contaminated residential soils: a field survey. Sci. Total Environ. 320, 245–257.
Gao, B., Gao, Y., Li, Y., 2010. Preparation and chelation adsorption property of composite chelating material poly(amidoxime)/SiO_2 towards heavy metal ions. Chem. Eng. J. 158, 542–549.
Ghasemi, M., Naushad, M., Ghasemi, N., Khosravi-Fard, Y., 2014. Adsorption of Pb(II) from aqueous solution using new adsorbents prepared from agricultural waste: adsorption isotherm and kinetic studies. J. Ind. Eng. Chem. 20, 2193–2199.
Hamdaoui, O., Naffrechoux, E., 2007. An investigation of the mechanisms of ultrasonically enhanced desorption. AICHE J. 53, 363–373.
Harter, R.D., 1983. Effect of soil pH on adsorption of lead, copper, zinc, and nickel. Soil Sci. Soc. Am. J. 47, 47–51.
Huang, Z.Y., Hong, X., Cao, Y.L., Chao, C., Zhi, Z., 2014. Assessing of distribution, mobility and bioavailability of exogenous Pb in agricultural soils using isotopic labeling method coupled with BCR approach. J. Hazard. Mater. 266, 182–188.
Junet, A.D., Basile, I., 2013. Characterisation of organic matter from organo-mineral complexes in an andosol from Reunion Island. J. Anal. Appl. Pyrolysis 99, 92–100.
Kadirvelu, K., Namasivayam, C., 2003. Activated carbon from coconut coirpith as metal adsorbent: adsorption of Cd(II) from aqueous solution. Adv. Environ. Res. 7, 471–478.
Kumar, M., Tripathi, B.P., Shahi, V.K., 2009. Crosslinked chitosan/polyvinyl alcohol blend beads for removal and recovery of Cd(II) from wastewater. J. Hazard. Mater. 172, 1041–1048.
Lützenkirchen, J., 1997. Ionic strength effects on cation sorption to oxides: macroscopic observations and their significance in microscopic interpretation. J. Colloid Interface Sci. 195, 149–155.
Meitei, M.D., Prasad, M.N.V., 2013. Lead (II) and cadmium (II) biosorption on *Spirodela polyrhiza* (L.) Schleiden biomass. J. Environ. Chem. Eng. 1, 200–207.
Park, D., Yun, Y.S., Park, J.M., 2010. The past, present, and future trends of biosorption. Biotechnol. Bioprocess Eng. 15, 86–102.
Ren, Y., Abbood, H.A., He, F., Peng, H., Huang, K., 2013. Magnetic EDTA-modified chitosan/SiO_2/Fe_3O_4 adsorbent: preparation, characterization, and application in heavy metal adsorption. Chem. Eng. J. 226, 300–311.
Sharma, Y.C., Sinha, A.S.K., Upadhyay, S.N., 2010. Characterization and adsorption studies of *Cocos nucifera* L. activated carbon for the removal of methylene blue from aqueous solutions. J. Chem. Eng. Datas 55, 2662–2667.
Sun, Y., Xie, Z., Li, J., Xu, J., Chen, Z., Naidu, R., 2006. Assessment of toxicity of heavy metal contaminated soils by the toxicity characteristic leaching procedure. Environ. Geochem. Health 28, 73–78.
Wang, G., Su, M.Y., Chen, Y.H., Lin, F.F., Luo, D., Gao, S.F., 2006. Transfer characteristics of cadmium and lead from soil to the edible parts of six vegetable species in southeastern China. Environ. Pollut. 144, 127–135.
Wang, L., Zhang, J., Zhao, R., Li, Y., Li, C., Zhang, C., 2010. Adsorption of Pb(II) on activated carbon prepared from *Polygonum orientale* Linn.: kinetics, isotherms, pH, and ionic strength studies. Bioresour. Technol. 101, 5808–5814.
Weber, W.J., Morris, J.C., 2015. Kinetics of adsorption on carbon from solution. J. Sanit. Eng. Div. 89, 53–55.
Yu, J., Huang, Z., Chen, T., Qin, D., Zeng, X., Huang, Y., 2012. Evaluation of ecological risk and source of heavy metals in vegetable-growing soils in Fujian province, China. Environ. Earth Sci. 65, 29–37.
Zhen, P.G., Zhi, F.Y., Tian, L.Y., Quek, S.Y., 2013. Adsorption isotherm, thermodynamics and kinetics studies of polyphenols separation from kiwifruit juice using adsorbent resin. J. Food Eng. 1, 195–201.